Precise Orbit Determination for NASA's Earth Observing System Using GPS

B. G. Williams
Navigation Systems Section

An application of a precision orbit determination technique for NASA's Earth Observing System (EOS) using the Global Positioning System (GPS) is described. This technique allows the geometric information from measurements of GPS carrier phase and P-code pseudo-range to be exploited while minimizing requirements for precision dynamical modeling. Briefly, the method combines geometric and dynamic information to determine the spacecraft trajectory; the weight on the dynamic information is controlled by adjusting fictitious spacecraft accelerations in three dimensions which are treated as first-order exponentially time-correlated stochastic processes. By varying the time correlation and uncertainty of the stochastic accelerations, the technique can range from purely geometric (for zero time correlation, infinite uncertainty) to purely dynamic (for infinite time correlation, zero uncertainty). Performance estimates for this technique as applied to the orbit geometry planned for the EOS platforms indicate that decimeter accuracies for EOS orbit position may be obtainable. The sensitivity of the predicted orbit uncertainties to model errors for station locations, non-gravitational platform accelerations, and Earth gravity is also presented.

I. Introduction

NASA's Earth Observing System will be a primary user of the Space Station polar platforms planned for the 1990s. The EOS project requirements have helped define the payload requirements for the polar platforms and have resulted in preliminary plans for three platforms to be flown concurrently in order to provide a long-term (10-year) data base of Earth science information. The platforms will carry a variety of remote sensing instruments, several of which will require or will benefit from precise orbit determination. These include a precision radar altimeter (similar in performance to the TOPEX altimeter), the High Resolution Imaging Spectrometer (HIRIS), and the Thermal Infrared Imaging Spectrometer (TIMS) [1].

The three platforms, referred to as platforms 1, 2, and 3, will be in near-circular, sun-synchronous orbits at 824 km altitude. The orbit of each platform will have a sixteen-day ground track repeat and will be near-polar. The orbit plane of platforms 1 and 2 will have its ascending node at 1:30 p.m. (local solar time, LST) on the Earth's true equator of date, while platform 3 will have its descending node at 9:30 a.m. (LST). The orbits of the three platforms differ only in their

phasing relative to the GPS constellation and the ground receivers being simulated in this analysis, and hence are essentially the same for the purposes of this preliminary covariance analysis. Of course, a more detailed mission design analysis for each platform would be concerned with the day-to-day variability in orbit uncertainties due to these phasing differences. With this in mind, platform 3 orbit parameters were used in this study to simulate geometry typical of all three platforms. The orbit parameters assumed for platform 3 were based on the current mission baseline design[1] and are presented in Table 1. The epoch time shown in Table 1 is arbitrary and was chosen to coincide with the epoch of existing trajectory predictions for the GPS constellation. The orbit node relative to the Earth true equator of date shown in Table 1 was chosen to place the orbit descending node at 9:30 a.m. (LST) on the epoch date.

The GPS tracking analysis techniques applied in this study are among several that have been developed at JPL over the past several years to probe the ultimate on-orbit precision available from GPS [2], [3], [4]. The techniques all require a GPS receiver aboard the spacecraft to be tracked and a precisely known global network of GPS ground receivers. The basis of these sub-decimeter GPS tracking strategies is their ability to exploit the extreme precision of carrier phase tracking by using it to smooth the geometric solutions obtained from the less precise pseudo-range measurements [3], [4]. The application of two of these techniques, the "non-dynamic" and "reduced-dynamic," to the determination of EOS orbits is the subject of this article. The reduced-dynamic method is the more robust of the two techniques, as will be shown in the results to follow. The reduced-dynamic method has been described in general for Earth orbiters as a method for exploiting the redundant geometric information available from GPS measurements while minimizing requirements for precision dynamical models. This technique is less sensitive to momentary viewing geometry between the EOS receiver and GPS, as are the non-dynamic methods, which eliminate orbit dynamics entirely [2].

This analysis used the **O**rbit **A**nalysis and **SI**mulation **S**oftware (OASIS), which was developed at JPL especially for studying GPS tracking performance over a wide range of applications [5]. OASIS capabilities include simulation/covariance analysis features for a variety of model parameters, including multi-spacecraft states and dynamic parameters, tracking station location parameters, media delay parameters, and a host of clock modeling parameters for both spacecraft and ground receivers. Any of these model parameters (except spacecraft states) may be treated as piecewise constant stochastic process noise in the filter. This flexibility of design allows the random clock behavior of GPS transmitters and receivers to be eliminated by modeling clock biases as uncorrelated stochastic processes at each measurement time. Also, the ability to model three-dimensional accelerations on EOS as exponentially time-correlated stochastic processes is the heart of the reduced-dynamic tracking technique. In this technique, the relative weighting of dynamics and geometry may be adjusted continuously by varying the a priori standard deviation and the correlation time of the stochastic acceleration. By selecting large a priori and steady-state standard deviations and a zero correlation time for these accelerations, the filter becomes the purely geometrical non-dynamic tracking technique.

The goal of this article is to demonstrate that if an advanced GPS receiver is flown on EOS (similar to the TOPEX GPS receiver) and if the data are processed correctly, then the orbit determination for EOS could achieve decimeter-level accuracies. This article outlines results from two differential GPS techniques and the system requirements that could be used to reach these decimeter-level accuracies. The study includes GPS tracking strategy for the EOS flight receiver as well as filter strategies and covariance results for short arcs of one and two orbits of EOS tracking.

II. Radio Metric Data Simulation

A. Simulation Assumptions

The data simulation assumed a fully operational GPS constellation consisting of eighteen GPS spacecraft, with three in each of six orbit planes. The orbit planes are inclined 55 degrees to the equator and are equally spaced 60 degrees apart in longitude. The three spacecraft in each orbit plane are equally spaced (120 degrees) and are phased 40 degrees from plane to plane to ensure global visibility (for ground sites) of at least four spacecraft. This is the anticipated configuration of the operational GPS assembly that is scheduled for completion sometime in 1990 [6].

As stated earlier, the orbit recovery methods used here require both a GPS receiver aboard EOS and a precisely known global network of ground GPS receivers. For this study, a worldwide network of ten GPS ground receivers was assumed with an a priori location uncertainty equal to 5 cm in each of three orthogonal directions. An elevation cutoff angle of ten degrees above the local horizon was also assumed for each ground receiver. A world plot showing the global distribution of these sites and the EOS orbit ground track for this study is presented in Fig. 1. It should be noted that the operation of the ground-based receiver network is completely independent of the EOS platform. These receivers make measurements only

[1] H. N. Norton (ed.), "EOS Phase A Final Report," JPL Report D-4566 (internal document), Jet Propulsion Laboratory, Pasadena, California, April 20, 1988.

to the GPS, and the improved GPS orbits are used to determine the EOS orbit indirectly. In fact, once such a global network is established, any number of other user spacecraft which are carrying GPS receivers could make use of the system for precision orbit determination with no impact on the network operation or on each other (assuming that processing is distributed to different host computers).

The GPS receiver aboard EOS was assumed to have the capability to track continuous carrier phase and P-code pseudo-range from five GPS spacecraft simultaneously through an antenna with a hemispherical field of view centered at the zenith; ground-based GPS receivers were assumed able to track up to eight spacecraft simultaneously. The measurement and timing precision requirements for the receivers are summarized in Table 2, along with other pertinent simulation assumptions. The measurement precision assumed for all receivers was 0.5 cm for carrier phase and 5 cm for pseudo-range over a five-minute integration time. This implies that the dual-frequency measurements have been combined to remove the first-order ionospheric delay. These requirements are within the expected capabilities of the next generation of GPS receivers being developed both for NASA's Deep Space Network and for flight aboard TOPEX in the 1990s.

B. EOS GPS Receiver Scheduling

In order to extract the maximum information from the GPS carrier phase observable, it is important that the receiver be able to continuously track each of the GPS dual-band carrier signals at 1.6 GHz and 1.2 GHz. The continuous count phase observable is ambiguous to an integer number of cycles of the carrier, which requires that an initial phase bias be solved for in addition to other state parameters. If the receiver momentarily loses "lock" and the continuous count is interrupted, then additional phase bias parameters must be estimated at each phase break. In general, when the number of phase breaks decreases, the solution strength increases because there are fewer parameters to estimate and because dynamic information is accumulated from continuous phase observables.

To show the importance of satellite selection and its impact on the non-dynamic tracking technique, the EOS flight receiver assumed for this study was capable of tracking only five GPS spacecraft simultaneously. Since EOS is in a near-polar, retrograde orbit, there is a sparsity of spacecraft to be tracked during some parts of the orbit. The number of GPS spacecraft visible to the assumed EOS antenna for the geometries assumed in this study is presented in Fig. 2. As seen in the figure, the number of visible spacecraft ranges from five to eight. For optimal tracking, the selection algorithm may have to trade off the geometrical strength of a particular configuration in favor of minimizing switching between the spacecraft. Excessive switching between GPS spacecraft could weaken the solution through the introduction of unnecessary phase breaks. Of course, there would be an advantage if the EOS receiver were assumed to be able to track all visible GPS, since then these scheduling trade-offs (and the corresponding receiver algorithms) would not be necessary.

The selection of which five GPS spacecraft to track at each measurement time over the two EOS orbits in this simulation was designed to maximize both the length of tracking for a given spacecraft and the geometric strength of the particular five tracked. In order to measure the geometric strength of a given GPS tracking selection, the Position Dilution of Precision [7], or PDOP, parameter was used. Small values of PDOP indicate good arrangements in the geometry and correspondingly small errors in position determination. Using tabular values of all possible PDOP values at each five-minute interval over the simulation, an iterative approach was used to select those five spacecraft at each measurement time which would give reasonably uninterrupted phase tracking with low or minimum PDOP values. The resulting tracks for each spacecraft were no shorter than ten minutes while some reached a maximum length of forty minutes; the average length was thirty minutes. The minimum values of PDOP that were available and the actual values for the tracking schedule used in this study are presented in Fig. 3. Overall, the tracking chosen here achieved the minimum PDOP values 30 percent of the time.

III. Performance Analysis

The simulated radio metric data described above were used to produce orbit covariance results for both the non-dynamic and reduced-dynamic filter strategies. In the sections that follow, the two techniques are compared for processing a single orbit of data, and then the processing is repeated for data arcs in which the geometric strength has been degraded. For this degraded case, it will be seen that the nondynamic solution degenerates sharply while the reduced-dynamic solution remains stable. Finally, some results for the reduced-dynamic filter strategy over arc lengths of two EOS orbits are presented.

A. Assumptions for Covariance Analysis

In each of the filter strategies presented here, all clock biases between receivers and GPS transmitters were solved for at each measurement time. This eliminates the effects of unstable oscillators which produce common systematic effects between receiver–GPS pairs, but the price that is paid is a loss of information and a reduction in geometric strength. Explicit double differencing of the data could be used to eliminate the clocks [2]; however, in the present analysis, this is done by

implicitly double differencing the data by modeling each clock bias as an uncorrelated stochastic process. Essentially, this modeling is equivalent to solving for a new clock bias at each measurement time. In this strategy, one clock is chosen as a reference and is not estimated; hence, all other clock offsets are relative to this master clock. Simulations and reductions of actual GPS radio metric data [8], [9] have demonstrated that these stochastic clock models give results comparable to explicitly double differenced data.

In both non-dynamic and reduced-dynamic strategies, the covariance of a pseudoepoch filter state was computed for each of the time "batches" over which the stochastic process noise parameters were assumed constant [4]. In this study, the batch length, Δt, was chosen to coincide with the measurement interval of five minutes. In other words, each batch is the same length and contains only one set of measurements from a given GPS/ground station set. The batches for the stochastic clock parameters coincided with those for the stochastic forces. These stochastic processes were characterized by correlation time, τ, a priori variance, σ_0^2, and steady-state variance, σ_p^2, which controlled the propagation of the variance, P_j, of the stochastic parameters from batch to batch (i.e., from time t_j to t_{j+1}) as follows:

$$P_{j+1} = m^2 P_j + \sigma^2 \tag{1}$$

where σ^2 is given by

$$\sigma^2 = (1 - m^2)\,\sigma_p^2 \tag{2}$$

with

$$m = \exp(-\Delta t/\tau) \tag{3}$$

In the case where $\tau \to 0$, Eq. (1) represents a white noise process with variance σ_p^2; as $\tau \to \infty$ it approaches a random walk process if σ remains non-zero. These concepts will be useful in considering the results to follow. The nature of the stochastic process representing the fictitious forces on EOS determines whether the filter strategy is non-dynamic ($\tau \to 0$, $\sigma_p \to \infty$) or dynamic ($\tau \to \infty$, $\sigma_p \to 0$). The reduced-dynamic technique combines these two strategies by proper choice of τ, σ_0, and σ_p. A mathematical description for this filter strategy in terms of a Kalman sequential filter formulation is presented in [4]. In the present study, both non-dynamic and reduced-dynamic techniques assume $\sigma_0 = \sigma_p$.

The filter states that were estimated for each of the strategies included the GPS spacecraft and EOS positions and velocities at epoch (114 parameters), the stochastic clock biases for each receiver (except the reference clock) and spacecraft clock (28 parameters), the phase ambiguity parameters between GPS transmitters and receivers for each data arc (97 parameters), and the stochastic acceleration on EOS (3 parameters) for a total of 242 estimated parameters. Furthermore, the orbit uncertainties presented here have been adjusted for mismodeled parameters. These "consider" sigmas take into account the a priori errors due to the following:

(1) Station location errors

(2) Troposphere delay for each of the ten ground receivers

(3) GM of Earth

(4) Gravity harmonics through 4th degree and order

(5) EOS solar pressure

(6) EOS atmospheric drag.

The a priori standard deviations of each of the estimated and considered parameters are given in Table 2.

The processing steps used for both the techniques studied involved filtering, smoothing, and mapping of both the estimate state computed covariance and the sensitivity of the estimate state to the considered parameters. First, the filter was used to compute covariance and sensitivity results for each batch in the data arc being processed. Next, these were smoothed, taking into account measurement data from all batches processed. Then these smoothed pseudoepoch results were mapped to each batch time in order to create "current state" results. These current state results are presented for both tracking techniques in the following sections.

B. Comparison of Two Filter Strategies

The results for non-dynamic processing of a single orbit of EOS tracking are presented in Fig. 4. In the figure, the consider uncertainty for each of three orthogonal components, the radial, cross-track, and down-track (or tangential), and the total Root-Sum-Square (RSS) of these components are plotted every ten minutes over the data span of one orbit (~100 min). The total number of measurements processed over this arc was 2,404, or 1,202 for each data type. This case assumed the stochastic acceleration on EOS had a steady state σ_p of 1.0 cm/sec^2 and a correlation time of zero. As will be demonstrated in the next section, the variations in uncertainty over time seen in Fig. 4 are the result of the momentary viewing geometry and the common visibility between EOS, GPS, and the ground receivers.

A reduced-dynamic strategy applied to the same one-orbit data arc produced the results shown in Fig. 5. In this case, the assumed stochastic acceleration on EOS had a σ_p = 2.0 μm/sec^2 and a correlation time of one day. Other reduced-dynamic

cases were run in which the steady state sigma on the EOS stochastic force was as small as 0.5 $\mu m/sec^2$ with essentially the same result. The result in Fig. 5 shows much smoother uncertainty in each component over the arc than was seen for the non-dynamic case; this is due to time correlation of position fixes through dynamics which are included in the reduced-dynamic scheme but which are removed entirely in the non-dynamic case. The larger error in radial component evident at the final time in both plots is due almost entirely to the considered station location error and is most likely due to an end of data arc effect rather than poor geometry, as it does not appear in the longer arc fit presented later.

The average error contributions for the two cases above are presented in Fig. 6. Each error source and the total RSS are displayed in Radial, Cross-track, and Down-track components, which are labeled as R, C, and D, respectively, in Fig. 6. The errors in this figure represent the root mean square (RMS) of each error source over the single orbit of data in the fit. The errors labeled "Data" in Fig. 6 are the formal error contributions due to the assumed measurement precision. Note that the station location error is the dominant error source in both techniques. As expected, the non-dynamic scheme showed very little sensitivity to mismodeled dynamic parameters with computed perturbations of less than 1 mm in each component due to those parameters. The only exception was a 2-mm radial perturbation due to Earth GM. The reduced-dynamic strategy showed slightly higher sensitivity to dynamic mismodeling, although the largest of these perturbations were less than 2 cm. The perturbations due to dynamic mismodeling for the reduced-dynamic case are presented in Table 3. Note that the largest of the dynamic perturbations in this case are due to gravity harmonics at about a centimeter or less. Further note that the maximum effect of atmospheric drag occurs in the down-track component, although it is still insignificant at 7.2 mm. Since the perturbations due to solar pressure and atmospheric drag were so small for both techniques, they were excluded from Fig. 6.

C. Performance With Degraded Tracking

In this section, the two techniques are compared over the same single-orbit fit as before, but the data arc was degraded in this case by deleting EOS measurements to three GPS spacecraft at 60 and 65 minutes past the epoch time. These two times correspond to the instances when a maximum of five spacecraft are visible as indicated in Fig. 2 at 0.60 and 0.65 orbit periods past epoch. Hence, only two spacecraft are being tracked by the EOS receiver at these times. This was done to simulate conditions that might occur if the selection algorithm in the GPS receiver aboard EOS fails to properly schedule tracking.

The results for the non-dynamic technique, shown for this case in Fig. 7, indicate a dramatic loss of solution strength where the geometric strength has been weakened. The errors computed for this case at other times in the orbit are essentially the same as those shown in Fig. 4, but errors computed for 60 minutes past epoch have increased to over 362 m. The error components at this time were dominated by the formal estimate error (362.2 m due to data noise); all the consider error contributions remained less than 30 cm. The size of the orbit error at the geometric singularity is determined by the a priori uncertainties on the state and the stochastic force; otherwise, the orbit error becomes infinite at these times. This behavior along with the recovery of the orbit for all times except the degraded time shows the essential point positioning nature of the non-dynamic scheme. It should be noted that the rapid loss of solution accuracy seen here can also occur if the ground network lacks sufficient common visibility to produce strong geometric information [2].

The results for reduced-dynamic processing of the degraded data are shown in Fig. 8. Now the errors are hardly perturbed at the 60-minute time point, and in fact the RSS error there has increased to only 13.3 cm compared to the 12.0 cm computed for the corresponding good geometry case of Fig. 5. The smoothing effect of the orbit dynamics has "carried" the solution past the geometric singularity to produce a good overall solution. This robustness of the reduced-dynamic strategy in the presence of momentary loss of geometric strength in the radio metric data contrasts sharply with the non-dynamic results shown in Fig. 7, and makes the reduced-dynamic technique the method of choice for precise GPS tracking.

D. Performance Over Longer Data Spans

In this section, the reduced-dynamic filter technique was applied to two orbits (~200 min) of the simulated data. This measurement arc was an extension of the single-orbit data arc analyzed above and contained an extra 2,300 measurements for a total of 4,704, or 2,352 of each data type. This case estimated the same parameters as the single-orbit cases except for an additional 14 phase biases which were due to extra GPS tracks in the longer arc. The a priori parameter uncertainties are again those listed in Table 2. Also, the stochastic acceleration on EOS was assumed to have a steady state sigma, σ_p = 2 $\mu m/sec^2$, and a correlation time of one day to be consistent with the single-orbit reduced-dynamic cases already presented. The results obtained for position errors in the two-orbit fit are presented in Fig. 9. The corresponding velocity errors for this case are shown in Fig. 10.

The error contributions for two-orbit results were also averaged over time and are presented in Fig. 11. Comparing this figure to reduced-dynamic errors for the single-orbit fit

shown in Fig. 6, note that the optimal filter (i.e., data noise) contribution is smaller for the two-orbit fit (~1.3 cm vs. ~2.3 cm), and that the sub-optimal filter error (i.e., consider error) in the radial direction has decreased slightly (by 0.74 cm RMS) over that obtained in the single-orbit reduced-dynamic case. However, the total error has grown slightly for the other two components by 1.51 cm RMS in cross track and 0.32 cm RMS in down track. These increased total errors are due to increases in the station location errors and troposphere errors. This counter-intuitive result is due to the sub-optimal filter behavior. Perturbations due to station location errors still dominate the solution, although the particular perturbation at 100 min past epoch is much smaller for the two-orbit case than for the single-orbit fit (compare Figs. 5 and 9). The perturbations due to atmospheric drag and gravity harmonics were slightly less than those in the single-orbit case, while for solar pressure and GM they either remained essentially the same or grew slightly; all the dynamic perturbations for this case are summarized in Table 4.

The slight increase in cross-track and down-track errors is due to weighting of the dynamic information relative to the geometric information which is a result of the particular values for τ and σ_p used in this study. The particularly large value of $\tau = 1d$ relative to the batch size, $\Delta t = 5$ min, may also be at fault since it results in $m = 0.9965$ from Eq. (3), and hence the fictitious forces were being modeled approximately as random walks. These random walk forces had little cumulative effect on the short single-orbit cases, but they could have influenced the errors in the longer two-orbit fit. Although these considerations of optimality merit further study, the results for the one- or two-orbit cases presented here both yield reduced-dynamic RMS errors of less than ten centimeters for each component.

IV. Conclusions

The EOS orbit can be determined to decimeter levels by GPS tracking if the EOS receiver takes full advantage of the precision inherent in the GPS signal. The GPS receiver aboard EOS should either be designed to receive signals from all GPS spacecraft in view, or be able to optimize selection for at least five spacecraft. In addition, this study assumed a ground network of ten GPS receivers distributed worldwide to ensure good common visibility of the GPS with the EOS receiver. This ground network was sufficient for the current analysis, but the optimal size and placement of such a network was not considered here. The establishment of any such network will certainly not fall entirely on EOS, however, since the tracking system will also be required by other precisely determined Earth orbiters in the 1990s (such as TOPEX). Sharing the network among many such users places no additional tracking burden on the system since the ground receivers track only the GPS.

Either of the data reduction techniques presented here can produce decimeter accuracy without precise dynamical modeling since they rely mainly on the geometric strength of the GPS measurements. However, the reduced-dynamic technique was the clear choice over the non-dynamic strategy whenever the geometric strength of the measurement data was degraded. Hence, this analysis presents reduced-dynamic GPS tracking as the best way to achieve EOS orbit accuracy without precise knowledge of orbit dynamical models.

Acknowledgments

The author wishes to acknowledge the help of P. J. Wolff, S. C. Wu, and T. P. Yunck in the preparation of this article.

References

[1] R. Hartle and A. Tuyahov, "The Earth Observing System," *Astrodynamics 1985; Proc. Conf., Pt. I*, 1986, pp. 529–550.

[2] T. P. Yunck and S. C. Wu, "Non-Dynamic Decimeter Tracking of Earth Satellites Using the Global Positioning System," paper AIAA-86-0404, AIAA 24th Aerospace Sciences Meeting, Reno, Nevada, January 1986.

[3] T. P. Yunck, S. C. Wu, and J. T. Wu, "Strategies for Sub-Decimeter Satellite Tracking with GPS," *Proc. 1986 IEEE Position, Location and Navigation Symp.*, November 1986, pp. 122–128.

[4] S. C. Wu, T. P. Yunck, and C. L. Thornton, "Reduced-Dynamic Technique for Precise Orbit Determination of Low Earth Satellites," AAS Paper 87-410, AAS/AIAA Astrodynamics Specialist Conf., Kalispell, Montana, August 1987.

[5] S. C. Wu and C. L. Thornton, "OASIS – A New GPS Covariance and Simulation Analysis Software System," *Proc. First Int. Symp. Precise Positioning with the Global Positioning System*, Rockville, Maryland, May 1985, pp. 337–346.

[6] B. W. Parkinson and S. W. Gilbert, "NAVSTAR: Global Positioning System – Ten Years Later," *Proc. IEEE*, vol. 71, no. 10, October 1983, pp. 1177–1186.

[7] R. J. Milliken and C. J. Zoller, "Principle of Operation of NAVSTAR and System Characteristics," in *Global Positioning System*, Washington, D.C.: The Institute of Navigation, 1980, pp. 3–14.

[8] S. C. Wu, S. M. Lichten, W. I. Bertiger, J. T. Wu, J. S. Border, B. G. Williams, and T. P. Yunck, "Precise Orbit Determination of GPS and Landsat-5," *Proc. Fourth Int. Geodetic Symp. Satellite Positioning*, Austin, Texas, 1986, pp. 275–288.

[9] S. M. Lichten and J. S. Border, "Strategies for High Precision GPS Orbit Determination," *J. Geophys. Res.*, vol. 92, no. B12, November 10, 1987, pp. 12751–12762.

Table 1. EOS orbit characteristics used in this study

Semi-major axis	7202 km	Longitude of ascending node,[a] Ω	143.1 deg
Eccentricity	0.00114	Argument of perifocus, ω	90.0 deg
Inclination[a]	98.7 deg	True anomaly	0.0 deg
Orbit period	101.4 min		

[a]Angles are referenced to Earth true equator and equinox of 21 March 1986, 14 h UTC.

Table 2. A priori standard deviations used in EOS study

EOS and ground GPS receiver performance	
Parameters	Standard deviations
Data noise	0.5 cm at 5-min interval, calibrated carrier phase
	5.0 cm at 5-min interval, calibrated P-code pseudo-range
Phase bias	1 sec
Clock bias	1 sec for receivers and satellites
Station location	5 cm each component
Zenith troposphere	1 cm
Spacecraft orbit uncertainty	
Parameters	Standard deviations
GPS state	2 m (X, Y, Z); 0.2 mm/sec (DX, DY, DZ)
EOS state	2 km (X, Y, Z); 2 mm/sec (DX, DY, DZ)
EOS accelerations	
Parameters	Standard deviations
Earth GM	0.004 km^3/sec^2
4 X 4 gravity	50% GEM10 – GEM10B
Atmospheric drag	20% uncertainty in C_D
Solar pressure	10% uncertainty in reflectivity

Table 3. Perturbations due to dynamic mismodeling for reduced-dynamic single-orbit case

Spacecraft position components	GM, cm	4 X 4 gravity, cm	Solar pressure, cm	Atmospheric drag, cm
Radial	0.18	1.22	0.08	0.20
Cross-track	0.10	0.73	0.04	0.18
Down-track	0.05	0.78	0.10	0.72

Table 4. Perturbations due to dynamic mismodeling for reduced-dynamic two-orbit case

Spacecraft position components	GM, cm	4 X 4 gravity, cm	Solar pressure, cm	Atmospheric drag, cm
Radial	0.31	1.03	0.09	0.10
Cross-track	0.14	0.72	0.06	0.14
Down-track	0.14	0.60	0.08	0.29

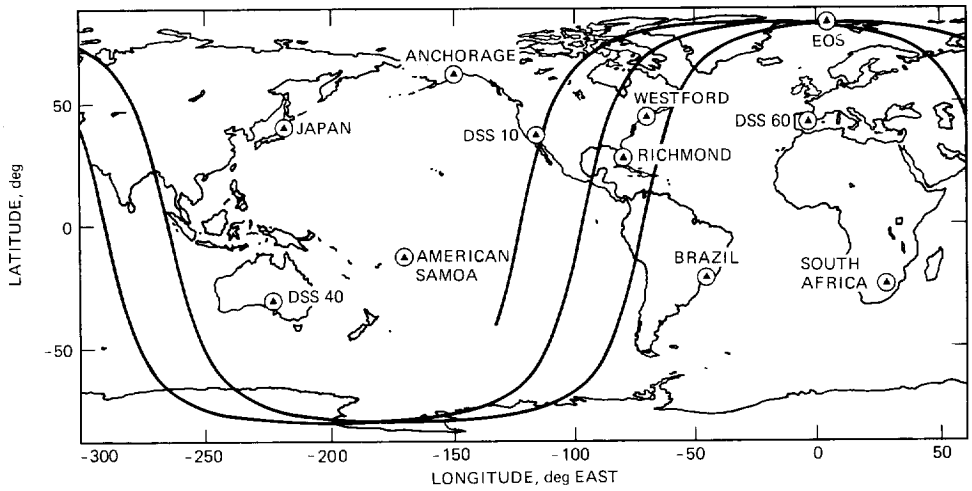

Fig. 1. Assumed worldwide network of GPS ground receiver locations and EOS orbit ground track

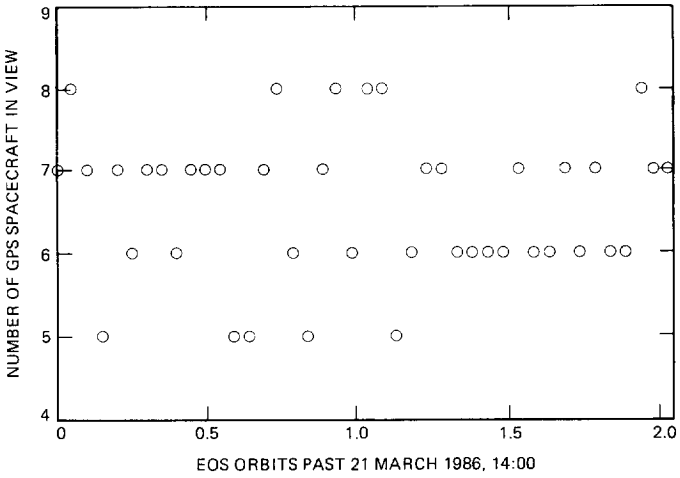

Fig. 2. Number of GPS spacecraft visible to EOS assuming a hemispherical field of view receiving antenna centered at zenith

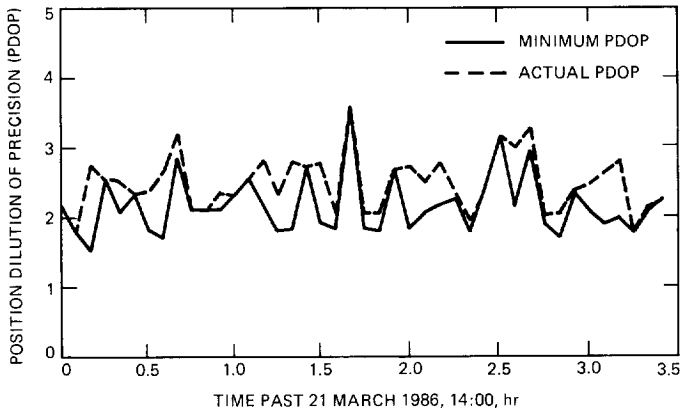

Fig. 3. Geometric strength of simulated EOS tracking; selection criteria maximizing length of track for a given GPS while minimizing PDOP

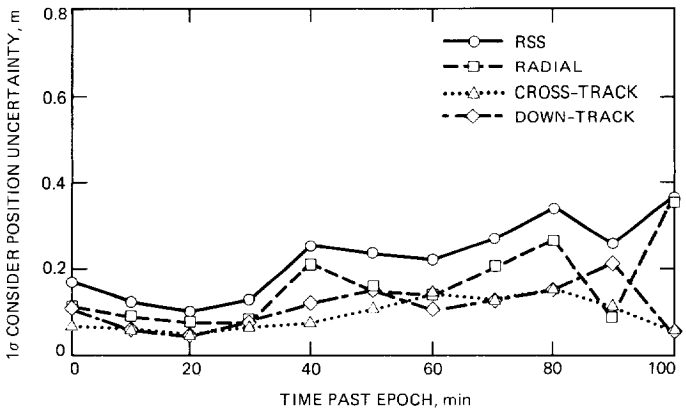

Fig. 4. EOS position uncertainty for non-dynamic tracking over one orbit

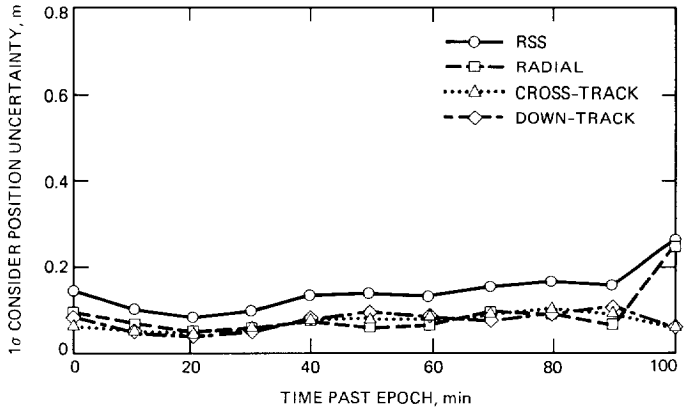

Fig. 5. EOS position uncertainty for reduced-dynamic tracking over one orbit

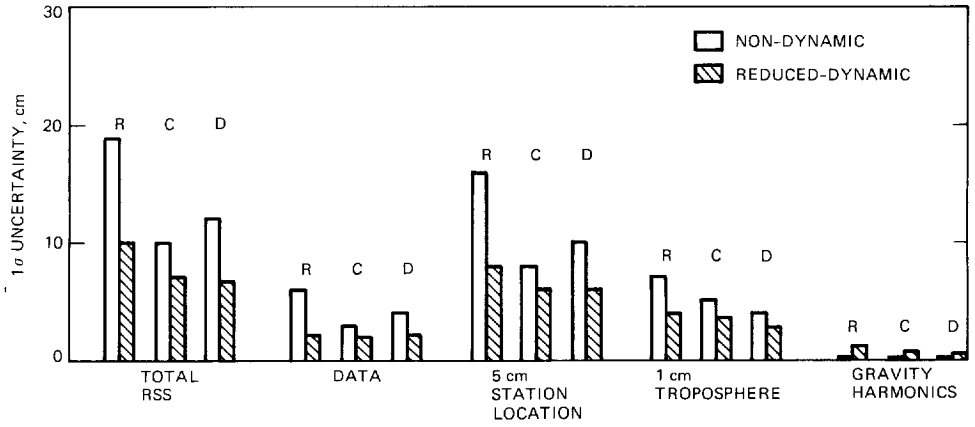

Fig. 6. EOS position error budget for both strategies; errors are RMS values over single-orbit cases of Figs. 4 and 5; R, C, D correspond to radial, cross-track, and down-track components

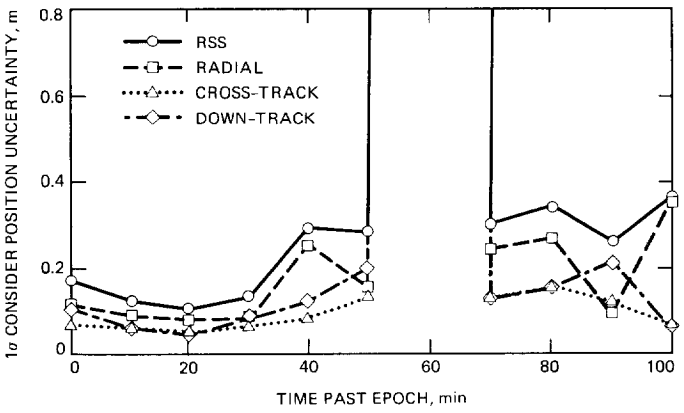

Fig. 7. EOS position uncertainty for non-dynamic tracking over one orbit; data deleted at 60 and 65 min to simulate bad GPS selection by EOS flight receiver

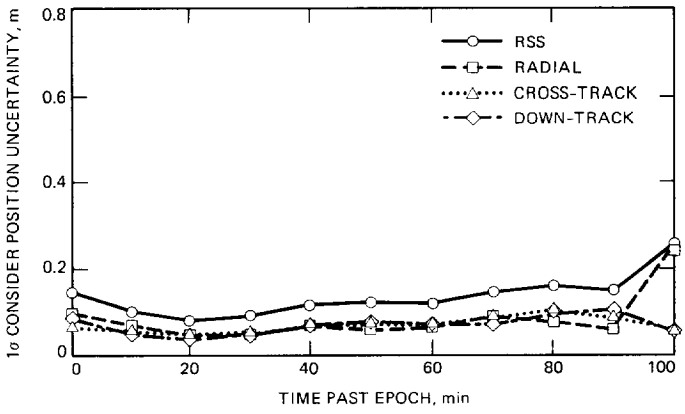

Fig. 8. EOS position uncertainty for reduced-dynamic tracking over one orbit; same measurement data as in Fig. 7

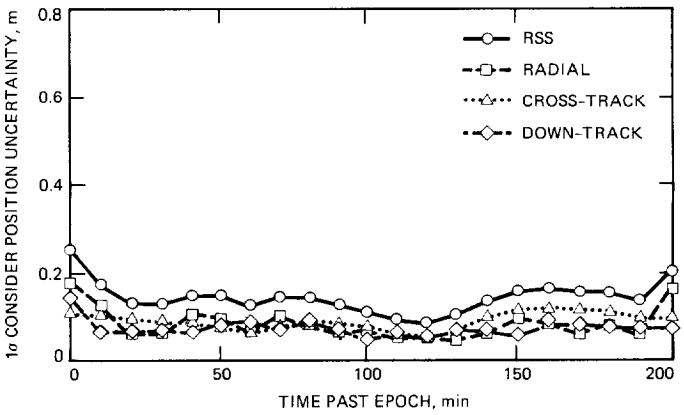

Fig. 9. EOS position uncertainty for reduced-dynamic tracking over two orbits

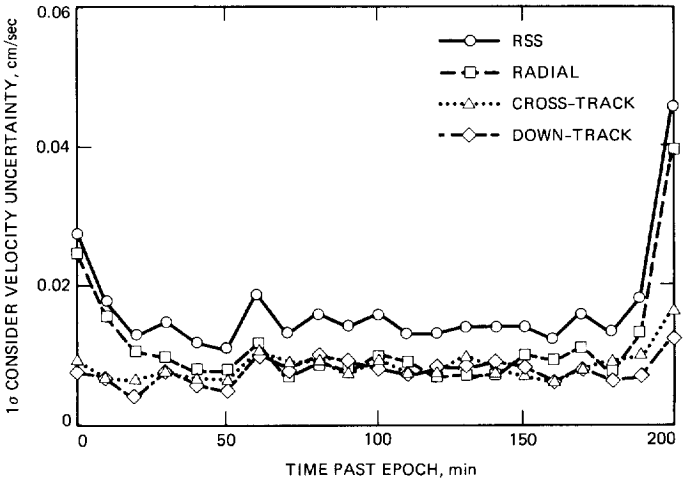

Fig. 10. EOS velocity uncertainty for reduced-dynamic tracking over two orbits

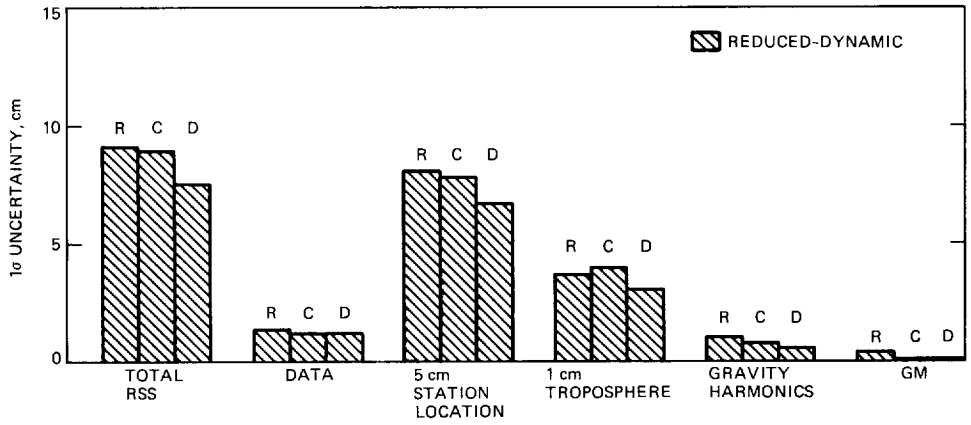

Fig. 11. EOS position error budget for reduced-dynamic tracking over two orbits; R, C, D correspond to radial, cross-track, and down-track components